Talbot- Lau interferometry with a non- binary phase grating for non-destructive testing

Yury SHASHEV [1], Andreas KUPSCH [1], Axel LANGE [1], Ralf BRITZKE [1], Giovanni BRUNO [1], Bernd R. MÜLLER [1], Manfred P. HENTSCHEL [2]
[1] BAM Bundesanstalt für Materialforschung und -prüfung, 12205 Berlin, Germany
[2] TU Berlin, Polymertechnik/Polymerphysik, 10587 Berlin, Germany

Contact e-mail: yury.shashev@bam.de

Abstract. Grating interferometric set-ups have been established in the last decade. They are promising candidates to obtain enhanced image contrast from weakly absorbing micro and nano structures. They are based on X-ray refraction and near-field diffraction using the Talbot effect.

At the expense of taking multiple images, Talbot-Lau grating interferometry allows separating the absorption, refraction, and scattering contributions by analysing the disturbances of a phase grating interference pattern. Contrary to other refraction enhanced methods, this technique can be applied using conventional X-ray tubes (divergent, polychromatic source). This makes it attractive to solve typical non-destructive testing problems.

We investigated the efficiency of phase gratings, i.e. the visibility (the amplitude of oscillations) upon variation of propagation distance and phase grating rotation around an axis parallel to the grid lines. This grating rotation changes the grating shape (i.e. the distributions of phase shifts). This can yield higher visibilities than derived from rectangular shapes.

Our study includes experimental results obtained from synchrotron radiation, as well as simulations for monochromatic radiation. The advantages of Talbot-Lau interferometry are demonstrated at the example of glass capillaries.

Introduction

In X-ray phase contrast imaging, the phase shift of the beam caused by the sample, is not directly measurable, but is converted to intensity variations, which are detected by the detector. The advantage of this method compared to the conventional absorption contrast X-ray imaging is a higher contrast, which allows seeing smaller details. But these methods require more complex devices, such as synchrotron or micro-focus X-ray sources, X-ray optics and high-resolution X-ray detectors. The most commonly used phase-contrast X-ray imaging techniques are the crystal interferometry [1], propagation-based methods [2], analyzer-based imaging (diffraction enhanced imaging [3]) and the grating based imaging [4]. The grating interferometry is based on the Talbot effect [5], a near-field diffraction effect. This self-imaging effect produces an interference pattern of a diffraction grating. At a certain distance (the so-called “Talbot distance”), this pattern gives exactly the structure of the grating, and is recorded by a detector. Talbot-Lau technique is a modern, non-destructive method that provides fast imaging access to interfacial properties of the materials. These features are made visible by enhanced phase contrast.

In this study, we investigate the efficiency (visibility) of phase gratings, which yields a phase contrast of the investigated materials. In the following sections, we will present, the Talbot- Lau interferometry set-up, the simulation of interference patterns and visibilities of phase gratings with varying of propagation distances and rotation of the grating around a vertical axis.

Using synchrotron radiation, we characterize phase gratings with different design energies upon of propagation distances. We will present how the visibility changes during rotation of the phase grating. Also, the simulation of a phase grating performance will be compared to experimental results. Finally, we will present absorption and dark field images of a first investigated sample (glass capillary).

2. Talbot-Lau interferometry

A typical grating-based interferometer set-up is sketched in figure 1. It is based on conventional radiography or tomography setup that includes an X-ray source, a sample and a detector. Additionally, two or three gratings (G0, G1, G2) are placed along the optical axis in the beam [6]. The first grating (G0, "source grating") ensures that the illumination of the actual interferometer gratings G1 and G2 has sufficient transverse coherence (parallel beam), which is a prerequisite for interference effects. When is using coherent sources, such as synchrotron sources, than G0 can be avoided.

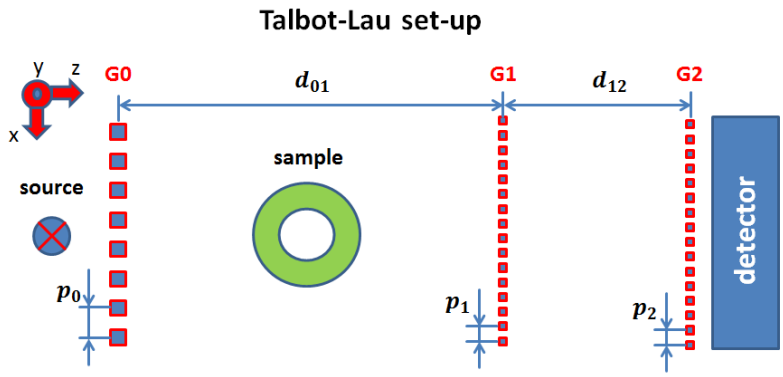

Fig. 1. Grating-based interferometer set-up (Talbot- Lau interferometer). G0- source grating with a period p_0, G1- phase grating with a period p_1, G2- analyze grating with a period p_2.

The (weakly absorbing) phase grating G1 is placed at distance d_{01} from G0 and modulates the phase of the radiation by a constant amount with the period p_1. Due the fractional Talbot effect [7] exist the phase shifts of the intensity pattern with the full or half period of the phase grating in excellent intervals behind G1. The phase grating used in our experiments has a duty cycle (ratio of bar width to grating period) of 0.5. The steps of (analyze or absorption) grating G2 with a period of (p_2) must have a half grating period of G1 (p_1/2) for a phase shift of π of the resulting intensity pattern. For a phase shift of π/2, the period is equal to p_1. The distances, at which these self-images are created, are called fractional Talbot distances. These distances depended on the phase shift caused by the G1, the wavelength λ of X-rays, and the phase grating period p_1. They base on the full Talbot distance Z_t which is given in a non-magnifying setup by the following formula (1):

$$Z_{t,n} = \frac{np^2}{16\lambda} \tag{1}$$

Here, n is the Talbot order. For a phase shift of $\pi/2$, maximum intensity modulation of G1 appear at fractions with n = 4, 8 etc. of full-lengths ($Z_t=2p^2/\lambda$) Talbot, and for a phase shift of π, at fractions with n = 1, 3 etc. For the laboratory construction, the G2 grating must be installed to one of these positions $d_{12}= Z_{t,n}$. The interference pattern itself has a period that is too small in general to be directly detected by a detector element (pixel). Nevertheless, the information about the changes in the interference pattern can be obtained. This is accomplished by laterally moving the analyzer grating in x-direction in multiple discrete steps; the intensity in each detector pixel is modulated sinusoidal. This procedure is called a stepping scan [8].

When a sample is introduced into the beam path, it modifies the interference pattern and thus the scanning curve in three ways: 1) Absorbing samples scale the scanning curve with a constant factor. From this change, the absorption contrast may be extracted. 2) Phase-shifting samples move the scan curve sideways. The displacement of the scanning curve reveals phase gradients of the sample. Changes of phase gradients of different values give a (differential) phase contrast. 3) Specimens with fine structures change the interference pattern locally in different directions and thus attenuate the amplitude of the scanning curve. Changes in this amplitude represent the dark-field contrast. The differential phase contrast and dark-field contrast have their origin in the same physical process: the refraction of X-rays.

3. Results

The results presented here are based on simulations of interference patterns (Talbot carpets) and measurements using synchrotron radiation at BESSYII in BAM*line*.

3.1. Simulation of Talbot carpets

Stacking interference patterns of as a function of distance creates the so-called Talbot carpets. In simulations, the radiation, in opposite to conventional X-ray absorption contrast is calculated as a wave field, rather than by simple geometrical optics. If a plane coherent X-ray wave hits the sample, the phase front behind the object is distorted. The simulations, used here, are based on the Huygens-Fresnel principle. The simulation includes a convolution of the point source and grating function. It was calculated in Mathematica 10.1 (Wolfram Research Inc.). For a phase grating made of 43.2 µm silicon bars, photon energies of 68 keV, 34 keV, and 11.33 keV, corresponding to $\pi/2$, π and 3π phase shifts. The corresponding detector distances were approximately Talbot distances Z_t, and the field of view in x direction is identical for all carpets (FOV_x = 79 µm). Thus, using a delta function can create a wave that will interact with the grating function. Fourier transformation of the grating function and delta function will be amplitude of fluctuation, and intensity is proportional to the mean square of the amplitude. As grating function we used two cases: rectangular and triangular shapes. In the figures 2 a), b) and c) are the Talbot carpets from the interaction delta function with a rectangular functions for 68 keV, 34 keV and 11.33 keV, respectively. Figures 2 d), e) and f) show the Talbot carpets from the interaction delta function with triangular functions for 68 keV, 34 keV and 11.3 keV, respectively. Simulations are presented for 3 periods with p=8 µm and approximately full Talbot propagation length.

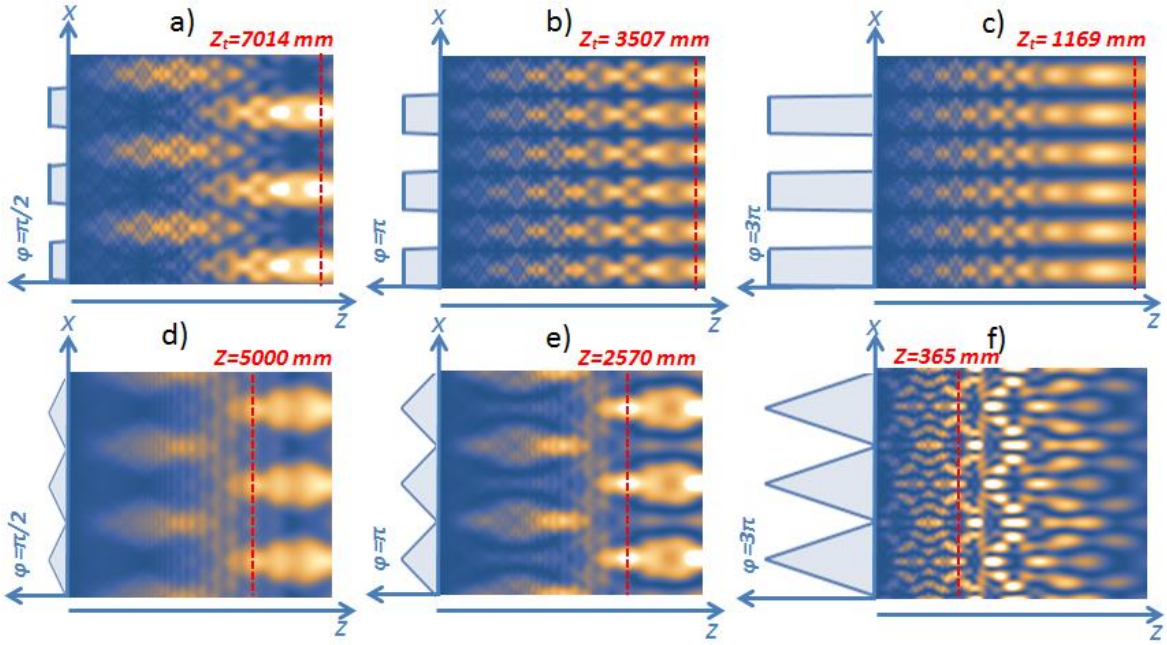

Fig. 2. Talbot carpets from the interaction delta function with a grating functions. a), b) and c) are the Talbot carpets from the interaction delta function with a rectangular function for energies 68 keV, 34 keV and 11.33 keV, corresponded $\pi/2$, π and 3π phase shifts. d), e) and f) are the Talbot carpets from the interaction delta function with a triangular function for 68 keV, 34 keV and 11.33 keV. Simulations present for 3 periods with p=8 μm and full Talbot propagation length.

For this simulation, we used increments in x direction Δx = 17.5 nm and in propagation length Δz = 10 mm. For the rectangular shape of phase shift of $\pi/2$, we generally generate patterns of period p_1. At $Z_t/2$ we observe a shift of intensity modulation by $p_1/2$, accompanied by increased intensity for $Z_t/2 < z < Z_t$. The same effect we can see for triangular functions (figure 2 d, e). Triangular shape of the phase grating give us an average phase shift (approximately at middle of the triangle height) approximately twice smaller than the rectangular phase grating with a same period. As an example, we compared Talbot carpet for the $\pi/2$- shifting rectangular phase grating (Fig. 2 a)) and the π-shifting triangular phase grating (Fig. 2 e)). For the π– and 3π- shifting phase grating in rectangular cases (figure 2 b, c), the interference patterns exhibit half the period of the grating, exclusively. It was calculated for the all rectangular gratings full Talbot distances and for all triangular gratings distances with a maximum intensity (dashed red lines). These simulated distances are in a good agreement with formula (1) calculated results and will be helpful for experiments on synchrotron and laboratory equipment.

3.2 Experimental results (synchrotron)

The phase grating G1 of period ~ 8 μm of height 43.2 μm and duty cycle 0.5 was prepared from a silicon wafer. For the characterization of the phase grating the following energies were used: 11.33 keV, 17 keV and 34 keV, corresponding to phase shifts of 3π, 2π and π, respectively. The height of the grating determines the phase shift.

The experiments are carried out at storage ring BESSY II at BAM*line*. The source of the beamline is a superconducting 7 T wavelength shifter (WLS) with energy resolution of ($E/\Delta E$ = 10^2 - 10^3) and stability 0.01%. As an optical element a Si (111) double-crystal monochromator for energies of about 5 keV to 50 keV and an energy bandwidth of about 0.2% is used [9]. The monochromatic beam is narrowed by a slit system to the field of view of about 1.7 × 1.2 mm^2. The imaging detector consists of a PCO 400 CCD-based camera of

4008 × 2672 pixels and magnifying optics, which results in an effective pixel size of 0.438 µm. The experimental set-up is sketched in figure 3 for high- resolution phase-contrast imaging. The many motorized degrees of freedom of the measuring station allow the continuous variation of different geometrical parameters.

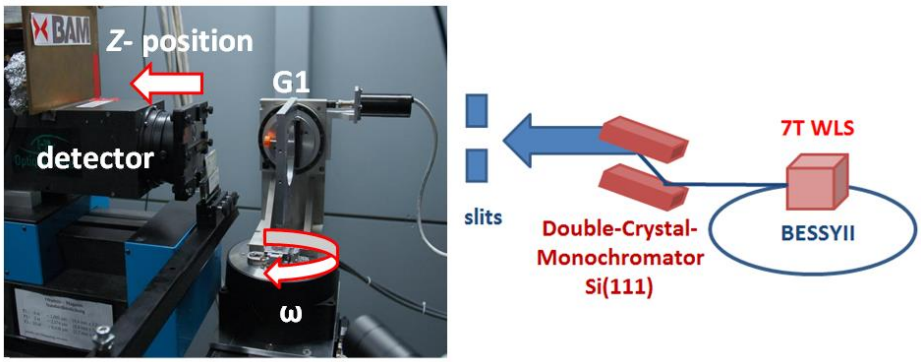

Fig. 3. Experimental equipment at storage ring BESSY II at BAM*line*.

In the first experiments, the distance between grating and detector is varied in the *z* direction (figure 5a). The above-mentioned energy detector scans are performed from 30 mm to 1000 mm in 10 mm increments.

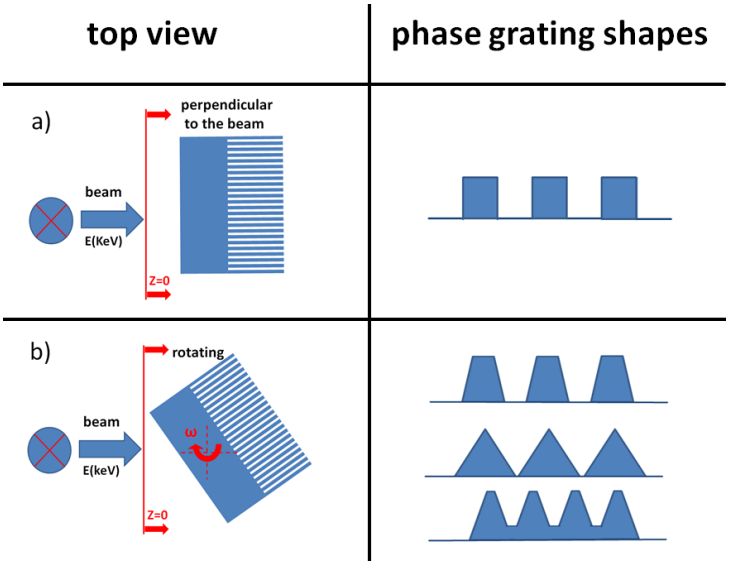

Fig. 4. Two types of experiments with variable grating – detector distances (top view) and phase grating shapes: a) grating is perpendicular to the beam (rectangular shape). b) Rotating the grating around the vertical axis at a certain detector distance. The grating shape changes form trapezoidal to triangular.

For the purpose of data correction, a so-called flat-field image (I_{flat}) and a dark-field image (I_{dark}) had to be recorded. They are used to modify the as-measured pattern (I_{mes}) according to

$$I_{corr}(z) = \frac{I_{mes}(z) - I_{dark}}{I_{flat}(z) - I_{dark}} \qquad (2)$$

From the corrected images (I_{corr}) one creates the interference patterns at different distances *z* (Talbot - carpet).

The so-called visibility (V) [4] serves as a contrast measure of the respective interference patterns. This defined as the modulation of the interference fringes relative to the base level and describes the efficiency of the phase grating. Mathematically, it is expressed by:

$$V = \frac{I_{max} - I_{min}}{I_{max} + I_{min}} \tag{3}$$

I_{max} – maximum intensity,
I_{min} – minimum intensity.

For the determination of the maximum visibility V, we conducted a second experiment. The phase grating has been rotated around the vertical axis (see figure 4b) in all certain detector distances (fractional Talbot distances). The angle of rotation ω was varied from -10° to 10° with increments $\Delta\omega$ = 0.5°. While for a rectangular grating shape the phase shift changes abruptly, for the triangle or trapezoidal shapes (non- binary grating shapes), the phase changes continuously. The visibility also changes as a function of rotation angle ω and energy. Experimental carpets with a period of phase grating p=8 µm, and corresponding visibilities depending on the rotation angle ω at the calculated first fractional Talbot distances are shown in Fig. 5 for 34 keV (black curve) a) and the third fractional Talbot distances for 17 keV (red curve) b).

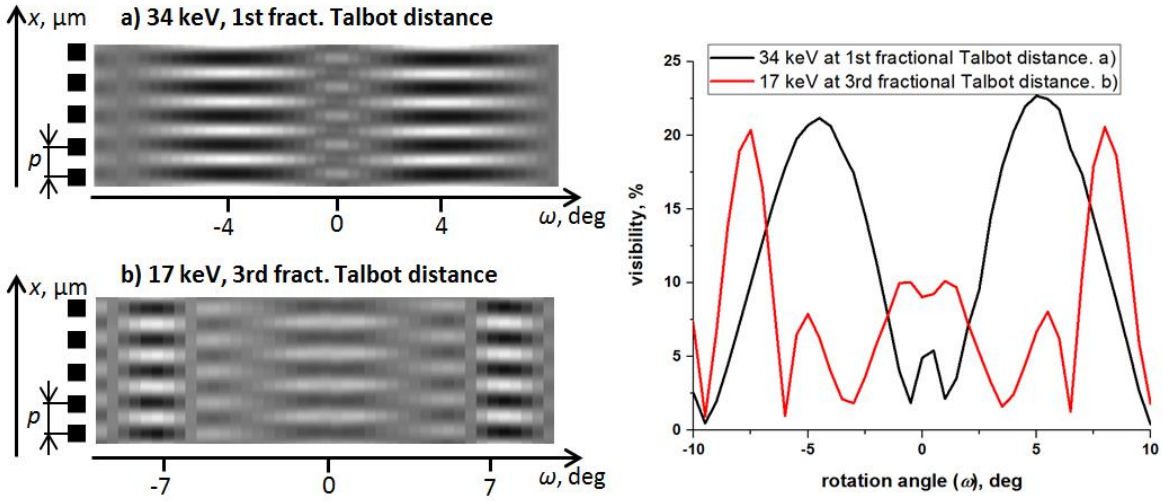

Fig. 5. Experimental carpets with a period of phase grating p=8 µm and corresponding visibilities as a function of rotation angle ω at a) the calculated first fractional Talbot distances for 34 keV (black curve), and b) the calculated third fractional Talbot distances for 17 keV (red curve).

As an outcome of the rotation experiment we performed detector distance scans at normal grating incidence and at angles where the maximum intensity modulations were observed. The experimental normal incidence carpets obtained at 17 keV and 34 keV are presented in figures 6 a, c, respectively, and carpets from 17 keV and 34 keV when the grating rotated by ω of 4° and 7° are shown in figures 6 b, d, respectively.

Yaroshenko *et al*. [10] observed an increase of visibility of discrete rotations of the phase grating about the vertical axis (parallel to the grating bars). Here, the rotation is experimentally investigated systematically. The curves in figure 6 e, are the interpolated visibilities from carpets presented in the figures 6 a,b,c,d. The blue (dotted) and black (solid) curves are the visibility modulations for 34 keV and 17 keV depending on the grating-detector distance (z) for the case that both gratings are perpendicular to the beam.

The pink (dashed-dotted) and red (dashed) curves are visibility modulations for 34 keV and 17 keV when the grating at an angle ω of 4° and 7° are rotated.

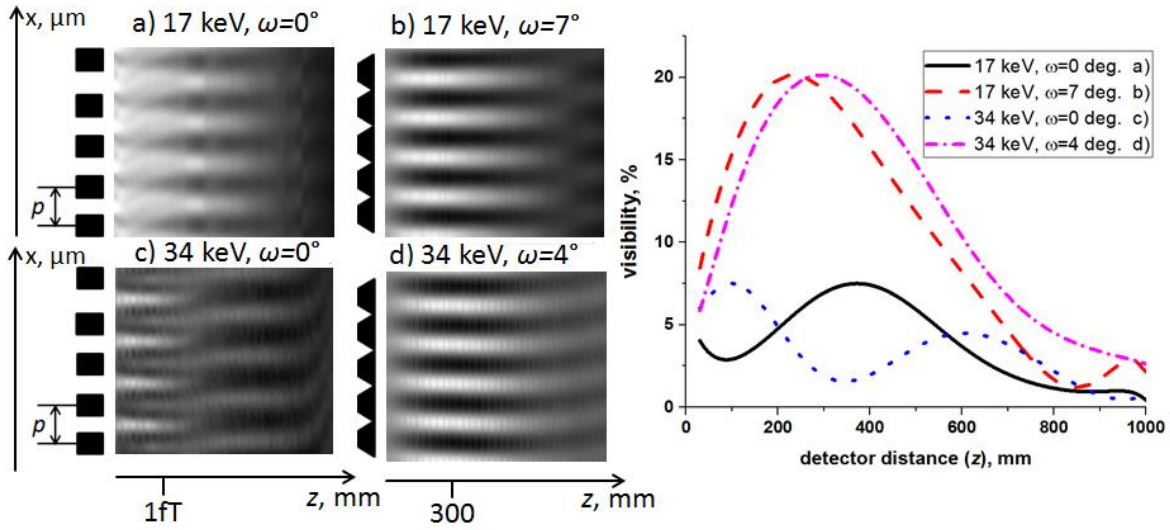

Fig. 6. Experimental carpets from 17 keV and 34 keV with a period of phase grating p=8 µm for the case: a), c) - gratings perpendicular to the beam (rectangular shape). 1fT- 1st fractional Talbot distance (for 34 keV, 1fT = 220 mm). b), d) - grating at an angle ω of 4° and 7° rotated (non-binary gratings). e) - interpolated visibilities from presented carpets.

The maximum visibility occurs in the case with energy of 17 keV and 7° at z = 250 mm, and in the case with energy of 34 keV and 4° at z =300 mm, and is 20%. This is significantly larger than for normal incidence. An interesting fact, in the experimental Talbot carpet for the π- shifting rectangular phase grating (Fig. 6 c), in the z propagation area approximately at 1st fractional Talbot distance (1fT) we observed the double frequency modulation with a decreasing visibility. Double frequency modulations are observed in the cases with minima visibilities and shifts of intensity modulation by p/2, which were observed in Talbot carpets in Fig. 5, as well.

4. Sample imaging

For the study and demonstration of phase contrast (dark- field imaging) using a grating interferometry was selected glass capillary (outer diameter 1 mm, inner diameter 0.7 mm). We used approximately triangle phase grating (grating rotate at 5.3°) with energy 11.33 keV. Images from 30 mm to 800 mm with increment 2 mm were acquired with an exposure time 20 second per step. The scans show sinusoidal intensity profiles with a period of 18 pixels with a detector resolution of 0.438 µm which corresponds to the full period of the phase grating. We performed two measurements: a reference measurement (without capillary) and a measurement with the capillary. The reference curve (blue) and modified by the object (red) are shown in Fig. 7a). Fig. 7b) reveals enhanced contrast close to walls for dark- field contrast imaging (DFC) compared to the for absorption contrast (AC) image due refraction and small angle scattering. Both images were recorded at the same grating-detector distance of 365 mm, what was simulated for a triangular function with a first maximum intensity (see figure 2f)).

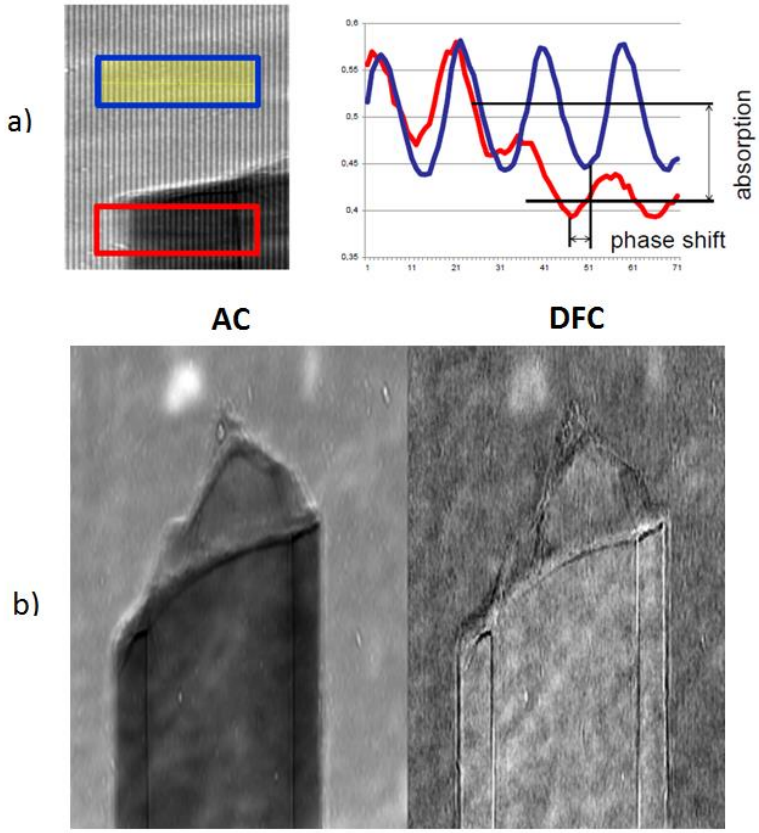

Fig. 7. a) Two scan profiles: blue- reference measurement, red- measurement with the object (1mm thick capillary). At the transition from flat field into the capillary a phase shift of 7 pixels is observed. b) Extracted images at 365 mm grating-detector distance: AC - absorption contrast, DFC - dark-field contrast.

Conclusion

Talbot-Lau grating interferometry allows separating the absorption, refraction, and scattering contributions by analysing the disturbances of a phase grating interference pattern. In this work, we presented how the efficiency of phase gratings can be improved for Talbot- Lau interferometry. By analysis of the pure phase grating interference pattern (Talbot carpets) we investigated the visibility depending on different parameters. We simulated Talbot carpets at different energies and two phase grating shapes (rectangular and triangular). For rectangular shapes, the obtained intensity maximum positions matched with the calculated fractional Talbot distances, whereas for triangular (trapezoidal) shapes those positions were shifted substantially. In the experiments we also achieved these shapes by rotation about the vertical axis (parallel to the grating). This rotation changes the distribution of phase shifts and yields higher visibility than for normal grating alignment (*i.e.*, ω = 0°). Two types of experiments were conducted to determine the visibility maximum – varying the propagation detector distance and varying the rotation angle. Comparison of experimental Talbot carpets and simulated carpets will be checked by the next study with more ideal phase gratings and with different energies.

Using non-binary phase grating, absorption and dark field image of a test sample (glass capillary) were presented.

References

[1] U. Bonse, M. Hart: An X-Ray Interferometer, Applied Physics Letters, **6** (1965) 155–156.
[2] A. Snigirev, I. Snigireva, V. Kohn, S. Kuznetsov, I. Schelokov: On the possibilities of x-ray phase contrast microimaging by coherent high-energy synchrotron radiation, Review of Scientific Instruments, **66** (1995) 5486–5492.
[3] D. Chapman, W. Thomlinson, R. E. Johnston, D. Washburn, E. Pisano, N. Gmür, Z. Zhong, R. Menk, F. Arfelli, and D. Sayers: Diffraction enhanced x-ray imaging, Physics in Medicine and Biology, **42** (1997) 2015-2025.
[4] C. David, B. Nöhammer, H. H. Solak, E. Ziegler: Differential x-ray phase contrast imaging using a shearing interferometer, Applied Physics Letters, **81** (2002) 3287–3289.
[5] H. F. Talbot: LXXVI.Facts relating to optical science. No. IV, Philosophical Magazine 3, **9** (1836) 401–407.
[6] F. Pfeiffer, T. Weitkamp, O. Bunk, C. David: Phase retrieval and differential phase-contrast imaging with low-brilliance X-ray sources, Nature Physics **2** (2006) 258–261.
[7] A. W. Lohmann: An array illuminator based on the Talbot-effect, Optik, **79** (1988) 41-45.
[8] T. Weitkamp, A. Diaz, C. David, F. Pfeiffer, M. Stampanoni, P. Cloetens, E. Ziegler: X-ray phase imaging with a grating interferometer, Optics Express **13** (2005) 6296–6304.
[9] A. Rack, S. Zabler, B. R. Müller, H. Riesemeier, G. Weidemann, A. Lange, J. Goebbels, M. Hentschel, W. Görner: High resolution synchrotron-based radiography and tomography using hard X-rays at the BAMline (BESSY II), Nuclear Instruments and Methods in Physics Research, **A 586** (2008) 327-344.
[10] A. Yaroshenko, M. Bech, G. Potdevin, et al.: Non-binary phase gratings for x-ray imaging with a compact Talbot interferometer, Optics Express **22** (2014) 547-556